The interrelations between microstructural evolution parameters and yield strength in underaged AA7xxx alloys – modelling and experimental analyses

Negar Baghbanaghaie, Alexis Deschamps, Michael Worswick, Shahrzad Esmaeili

The interrelations between microstructural evolution parameters and yield strength in underaged AA7xxx alloys – Modelling and experimental analyses

N. Baghbanaghaie, A. Deschamps, M.Worswick, S. Esmaeili
University of Waterloo, 200 University Ave. West, Waterloo, ON, Canada N2L 3G1
University of Grenoble Alpes, CNRS, Grenoble INP, SIMaP, F-38000 Grenoble, France

Abstract

A new microstructural evolution model is developed to relate the evolution of precipitate size during underaging to its relative volume fraction for concurrent precipitate nucleation and growth processes. By combining the new microstructural model with a previously developed yield strength model, a new formulation is also developed to predict precipitation hardening due to weak shearable precipitates as a function of only a single variable. A combination of small angle x-ray scattering (SAXS), isothermal calorimetry (IC) and microhardness measurements is used to evaluate and validate the new models.

Keywords: Aluminum alloys, Precipitation, Modeling, Calorimetry, Small angle x-ray scattering (SAXS).

AA7xxx alloys are widely used for structural applications by the aerospace industry for their combination of low density and high strength, due to their precipitation hardening behavior, as well as their corrosion resistance and other mechanical properties [1]–[3]. These alloys are also of interest for automotive applications due to the demand for lightweighting and enhanced performance of personal vehicles [4]. AA7xxx alloys are commonly used in the thermomechanically-processed and overaged condition for aerospace applications, while for automotive applications, new design strategies and criteria based on cost-effectiveness (*e.g.* aging during paint bake cycling, PBC) will be needed. The evolution of hardening precipitates

during aging in AA7xxx alloys has been experimentally studied using various methods. In particular, small angle x-ray scattering (SAXS) has been found to be an effective tool for characterizing the time/temperature-dependence of microstructural evolution during aging [1], [5]–[13]. Equally effective, calorimetry approaches, particularly isothermal calorimetry (IC) analyses, have enabled characterization of the evolution of the relative volume fraction of precipitates (f_r), and thus the kinetics of precipitation, during underaging in 6000 and 7000 series Al alloys [14]–[18]. The precipitation kinetics data, in combination with precipitation hardening modelling approaches, has previously enabled reliable modelling of commercially-important age hardening processes [15]–[18]. The current investigation aims to further advance those modelling approaches by (a) formulating the interrelation between the average precipitate size (r) and the relative volume fraction of precipitates (f_r) for nucleation-affected growth underaging processes, and (b) developing a new single variable model that enables reliable predictions of precipitation hardening due to the evolution of the so-called "weak obstacle" shearable precipitates [16]–[18]. The validity of the new modeling relations is verified through comparison of the model predictions with the results from (a) SAXS and IC measurements of microstructural evolution, and (b) microhardness and yield strength (YS) data for hardening during multi-step aging of AA7030 and direct artificial aging of AA7050.

Precipitation hardening in underaged conditions commonly involves concurrent precipitate nucleation and growth [19]–[22]. Accordingly, the increase in the relative volume fraction of precipitates is related to the increase in both number density, N, and the volume of an average-size precipitate, $\bar{V}$. The change in f_r is, therefore, modeled as:

$$f_r = \frac{V_{ppt}}{V_{total}} = \frac{N\bar{V}}{V_{total}} \quad (1)$$

where V_{ppt} and V_{total} are the volume of precipitates per unit volume of the alloy at time *t* and at the peak aged condition, respectively. Assuming a spherical morphology for the precipitates (*i.e.,* $\bar{V} = \frac{4}{3}\pi r^3$), and considering the changes in f_r, *N*, and *r* during an increment in aging time, *dt*, as df_r, dN and dr, respectively, Eq. (1) can be re-written as:

$$\frac{df_r + f_r}{f_r} = \left(\frac{dN+N}{N}\right)\left(\frac{dr+r}{r}\right)^3 \quad (2)$$

Expanding Eq. (2) and neglecting the smallest multiplicative products of $\left(\frac{dr}{dt}\right)^3, \left(\frac{dr}{dt}\right)^2, \frac{dN}{N} \times \left(\frac{dr}{dt}\right)^3, \frac{dN}{N} \times \frac{dr}{dt}, \frac{dN}{N} \times \left(\frac{dr}{dt}\right)^2$ results in:

$$\frac{df_r}{f_r} = \frac{dN}{N} + 3\frac{dr}{r} \quad (3)$$

Additionally, following Deschamps and Brechet [19]:

$$\frac{dN}{N} = \frac{dr}{r_* - r} \quad (4)$$

In general, the radius of the critical nucleus, r^*, is inversely proportional to the driving force for nucleation ($r^* \propto \frac{1}{\Delta G_v}$) [19], [23]. For underaging conditions with high matrix supersaturation, it can be assumed that the large ΔG_v results in $r^* \approx 0$. Simplifying Eq. (3) by using Eq. (4) and the above assumption, and then integrating, results in the following relationship between r and f_r:

$$r = r^c \sqrt{\frac{f_r}{f_r^c}} \quad (5)$$

The parameters r^c and f_r^c are the average size and relative volume fraction of precipitates for a known underaged state, respectively, with $0 \leq f_r < f_r^c \leq 1$, $0 \leq r < r^c \leq r_{peak}$, and r_{peak} being the average radius of precipitates for the peak-aged condition. The limits of $f_r = 0$ and $f_r = 1$ correspond to the as-quenched (AQ) and peak-aged conditions [17].

Eq. (5), denoted as the "nucleation-affected precipitate growth" model, enables modelling of the yield strength (YS) as a function of a single microstructural variable, *i.e.* f_r (or r) for underaging processes that involve the formation of weak shearable obstacles. The basis of the YS modelling is the approach developed by Esmaeili *et al*. [17], according to which precipitates, as obstacles to dislocation movement, are considered "weak" when the dislocation breaking angle at the obstacle is larger than 120°. The contribution of such precipitates to the YS, σ_y, is given by [16]:

$$\sigma_{ppt|Weak} = C_1(f_r)^{1/2}(\frac{r}{r_{peak}})^{1/2} \qquad (6)$$

in which parameter C_1 is the scaling factor associated with the YS at the peak-aged condition [16]. Now by replacing Eq. (5) in Eq. (6), considering $r^c = r_{peak}$ and $f_r^c = 1$, a single-variable hardening model is obtained, as follows:

$$\sigma_{ppt|Weak} = C_1(f_r)^{3/4} \qquad (7)$$

The evolution of f_r during non-isothermal underaging from an initial value of f_r^0 to unity at the peak-aged condition is modeled according to the formulation developed by Esmaeili and Lloyd [15]:

$$f_r = 1 - (1 - f_r^0)\, exp[-\textstyle\sum_i k_i^n (t_i^n - t_{i-1}^n)] \qquad (8)$$

The parameter *n* in Eq. (8) is a time exponent mostly defined as a shape factor and k_i is the rate constant which has an Arrhenius relationship with temperature [15]:

$$k_i = k_0 exp\,(\frac{-Q_a}{RT_i}) \qquad (9)$$

where k_0, Q_a, and R are the proportionality constant, an activation energy term, and the universal gas constant, respectively [15].

The YS of the underaged alloy is then predicted by the linear addition of the strengthening contributions from the intrinsic strength of the matrix, σ_{int}, solid solution, σ_{ss}, and precipitation

σ_{ppt} [17]:

$$\sigma_y = \sigma_{int} + \sigma_{ss} + \sigma_{ppt} \quad (10)$$

where σ_{ss} is defined as:

$$\sigma_{ss} = \sigma_{0ss}(1 - f_r)^{2/3} \quad (11)$$

The constant parameter σ_{0ss} is the contribution from solid solution to the YS in the fully-supersaturated, *i.e.* as-quenched (AQ), state of the alloy for which $f_r = 0$.

Experimental evaluations were conducted on two aluminum alloys, AA7030 and AA7050 (Table 1). A summary of the heat treatment routes and the experiments conducted on the two alloys is presented in

Table 2.

Table 1. Chemical composition of AA7030 and AA7050 used for the modeling validation (%wt).

Alloy	Si	Mg	Ti	Cu	Zn	Fe	Zr	Manufacturer
AA7030	-	1.22	-	0.3	5.45	-	-	Hydro-Raufoss [24]
AA7050	0.03	2.04	0.02	2.15	6.44	0.04	0.11	Arconic

Table 2. Summary of the testing conditions of AA7030 and AA7050 alloys.

Method	**AA7030**			**AA7050**	
	Heat treatment		Identifier	Heat treatment	Identifier
Solution treatment (SHT)	20 min at 480°C (classical furnace) + water quenching (WQ)		AQ	10 min at 470°C (sand bath furnace) + WQ	AQ
SAXS	A	**Initial condition**: SHT + 24h NA	NA	--------	--------
		Step 1 SAXS: 5°C/s to 100°C + 5h at 100°C	PA		
		Step 2 SAXS: 5°C/s to 150°C + 8h at 150°C	--------		
	B	**Initial condition:** SHT + 1h NA	NA		
		Step 1 SAXS: 5°C/s to 100°C + 5h at 100°C (PA)	PA		
		Step 2 SAXS: 5°C/s to 130°C + 15min at130°C	--------		
		Step 3 SAXS: 6°C/min to 170°C + 2 h at 170°C	--------		

IC	**Initial condition**	SHT+24h NA +5h at 100°C	PA	SHT	AQ
	Aging during IC	t at 130, 150, or 170°C [25].	--------	t at 135, 150, 165, 177, 190°C.	--------
Mechanical testing	**Initial condition**	SHT+ 24h NA+ 5h at 100°C	PA	SHT	AQ
	Aging	Final-state aging at 150°C (YS data obtained from reference [24]).	--------	Aging at 150°C (Microhardness tests)	--------

*Note: AQ: as-quenched, NA: naturally-aged (aged at room temperature), PA: pre-aged,
For the IC tests, t was selected as the time required to achieve peak strength.

The details of the SAXS measurement methodology can be found in references [26], [27]. The experiments were conducted on a rotating anode with a Cu target and the X-ray intensity scattered by the precipitates was recorded. The recorded intensity allowed the measurement of the average precipitate radius r using the self-consistent procedure for Guinier radius determination presented in references [11], [27], as well as the integrated intensity Q, at underaging time t [26]. Considering that the integrated intensity is a representative of the precipitate volume fraction [12], f_r values through SAXS were estimated as $f_r \approx \frac{Q}{Q_{peak}}$, in which Q_{peak} represented the integrated intensity at the peak-aged condition. IC tests were conducted using a SETARAM C80 apparatus. The IC procedure for the AA7030 and AA7050 can be found in references [16] and [28], respectively. In both cases the repeatability of the results was confirmed by running multiple tests on each heat treatment condition. IC data was analysed to obtain the kinetic parameters for modelling of f_r (Eq. (8)) as a function of artificial aging time and temperature. The IC data analysis details are included as a flow chart in the Supplementary Material.

Vickers microhardness measurements were conducted using a Leco micro-hardness tester (300 g) load to obtain the experimental data for the YS of the AA7050 according to the commonly

used approximation $\sigma_y\ (MPa) \sim H_v \times 3$ [19]. At least five measurements were done on each sample and the average values were converted to YS.

The nucleation-affected growth model is evaluated by implementing Eq. (5) on AA7030 in two ways: (I) using the experimental values of r^c, f_r^c, and f_r, and (II) using the experimental values of r^c, and the modeling values of f_r^c and f_r obtained from equations (8) and (9), and the corresponding kinetic parameters found from the analysis of IC data. The procedure to obtain the kinetic parameters, as listed in Table 3, are outlined in the Supplementary Material. The constant values of r^c and f_r^c for the above evaluations are obtained for the sequential underaging states as follows: (a) route A: steps 1 and 2, in which the superscript c represents 5h at 100°C, and 8h at 150°C (peak-aged condition), respectively, and (b) route B: steps 1, 2, and 3, in which, the superscript c represents 5h at 100°C, 15 min at 130°C, and 2h at 170°C (peak-aged condition), respectively.

The results of evaluation I and II, along with the corresponding experimental data, for routes A and B conducted on AA7030 are shown in Figure 1 (a) and (b), respectively. As part of evaluation (II), the predicted f_r values are also compared with the f_r values obtained from SAXS data for aging routes A and B, with the results shown in Figure 1 (c) and (d), respectively.
It is clear that in both aging routes, the experimental and modeling results agree well. The maximum discrepancy between the modeling and experimental results of precipitate radius, is observed in Figure 1 (a), after 7 minutes of aging at 150°C in route A, *i.e.* ~ 20%. This level of discrepancy could be due to ignoring the potential dissolution of a small fraction of pre-aging precipitates at the initial stages of aging [11]. The evaluation results, thus, confirm the validity of Eq. (5), as well as the applicability of Eqs. (8) and (9) to model the evolution of f_r. In addition, the results suggest that SAXS and the current kinetic modelling methodology, which draws its

constant parameters from the IC analysis, may be interchangeably used for the quantification of microstructural evolution during non-isothermal underaging of AA7xxx alloys.

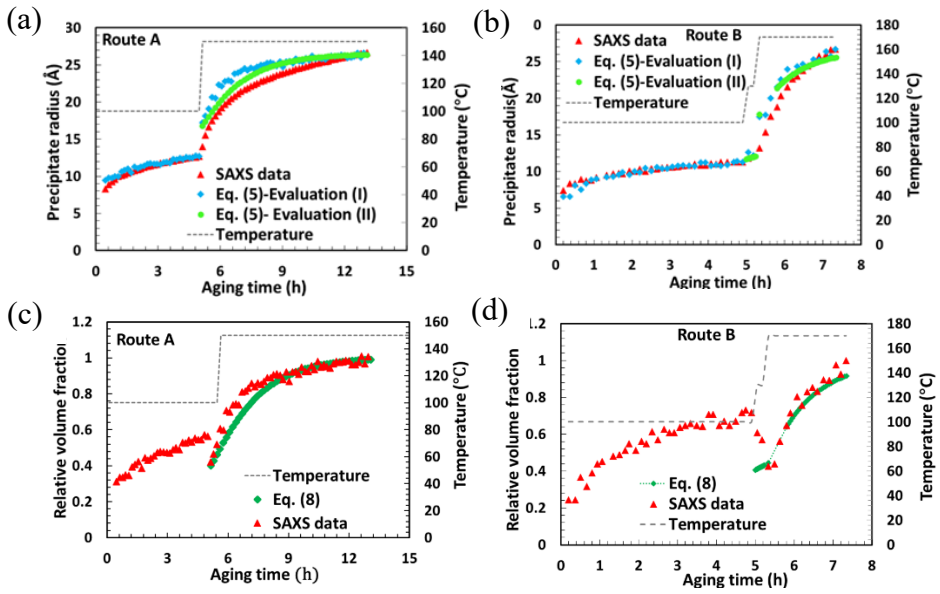

Figure 1. Comparison of the measured and predicted values of (a) and (b) precipitate radius r, and (c) and (d) f_r values, for AA7030 during aging at routes A and B, respectively.

The modified weak obstacle strengthening model (Eq. (7)) is evaluated by comparing the YS modelling results with the YS data reported for AA7030 in reference [24], and the measured hardness values of AA7050. The model calculations require the predicted f_r values (Eqs. (7) and (11)), and the calibration parameters σ_{0ss} and C_1. The latter are obtained using the YS data for the AQ and the peak-aged conditions of the two alloys, respectively (see Table 3), according to the procedure outlined in references [15], [17]. The predicted f_r values are obtained by implementing equations (8) and (9) and using the IC data. The detailed procedure for obtaining the calibration (*i.e.* constant) parameters for f_r calculation is shown in the flow chart in the Supplementary Material. The calibration parameters are listed in Table 3. The YS model prediction results, along with the corresponding experimental data, for the final-stage artificial aging of the AA7030-PA, as well as the direct artificial aging of the AA7050-AQ are presented in Figure 2 (a) and (b), respectively. It can be observed that modeling according to Eq. (7)

provides excellent predictions for the YS in both cases. This result suggests that the new weak obstacle model is capable of predicting the yield strength evolution during artificial aging of AA7xxx alloys regardless of their aging history.

Table 3. Calibration parameters used for the kinetic and the YS models for AA7030 and AA7050 alloys.

Parameter		f_r^0	n	$k_0(\frac{1}{s})$	$Q_a\ (\frac{kJ}{mol})$	$C_1(MPa)$	$\sigma_{0ss}(MPa)$	$\sigma_i(MPa)$
Value	AA7030 (PA)	0.4	1.1	2.3×10^3	59	389*[24]	50* [24]	10
	AA7050 (AQ)	0	0.8	3.6×10^2	48	533	125	10

*Note: These values are calculated using the YS data reported in reference [24].

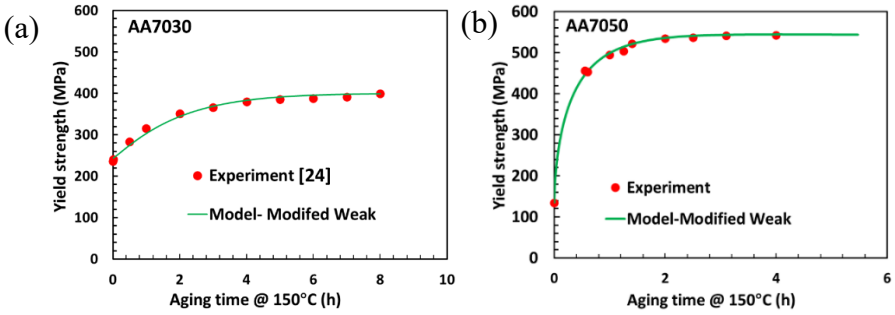

Figure 2. Comparison of the modeling and experimental YS results of (a) the PA AA7030 during final-state of aging at 150°C, and (b) the as-quenched AA7050 during aging at 150°C.

In summary, a model has been developed to predict the precipitate size as a function of the relative volume fraction of precipitates during underaging processes which undergo concurrent nucleation and growth of precipitates. Using the new precipitate size model, the precipitation strengthening formulation for weak obstacles has been advanced to enable the calculation of the YS as a function of a single variable f_r. The models have been validated by the excellent agreement between the predicted values and the experimental results. Additionally, the f_r values obtained from the current kinetic modelling approach and IC analysis have been compared with the results from SAXS measurements. The excellent agreement between the two sets of results suggests that these different methodologies may be interchangeably used for the quantification of microstructural evolution during non-isothermal underaging of AA7xxx alloys.

Acknowledgements

The financial support of this work was provided by Honda R&D Americas Inc., Arconic Ground Transportation Group, Promatek Research Centre, the Natural Sciences and Engineering Research Council (NSERC), the Canada Foundation for Innovation, the Ontario Research Fund, the Ontario Centres of Excellence, and the Ontario Advanced Manufacturing Consortium. The authors wish to extend their appreciation to Prof. Warren Poole for the provision of the AA7030 material and Prof. P. Sepehrband for the IC tests she had conducted on AA7030 alloy.

References

[1] J. . Werenskiold, A. Deschamps, and Y. Brechet, *Materials Science & Engineering A*, vol. 293, no. 13, pp. 267–274, 2000.

[2] P. Guyot and L. Cottignies, *Acta Materialia*, vol. 44, no. 10, pp. 4161–4167, 1996.

[3] L. M. Cheng, W. J. Poole, J. D. Embury, and D. J. Lloyd, *Metallurgical and Materials Transactions A: Physical Metallurgy and Materials Science*, vol. 34 A, no. 11, pp. 2473–2481, 2003.

[4] R. S. Long, E. Boettcher, and D. Crawford, *JOM*, vol. 69, no. 12, pp. 2635–2639, 2017.

[5] G. E. Totten and D. S. MacKenzie, *Handbook of Aluminum: Volume 2: Alloy production and materials manufacturing*. CRC press, 2003.

[6] L. Couturier, A. Deschamps, F. De Geuser, F. Fazeli, and W. J. Poole, *Scripta Materialia*, vol. 136, pp. 120–123, 2017.

[7] A. Deschamps, F. Bley, F. Livet, D. Fabregue, and D. J. Lloyd, *Philosophical Magazine*, vol. 83, no. 6, pp. 677–692, 2003.

[8] A. Deschamps, Y. Brechet, and F. Livet, vol. 15, pp. 993–1000, 1999.

[9] D. Liu *et al.*, *Materials Science and Engineering A*, vol. 588, pp. 1–6, 2013.

[10] Z. W. Du, Z. M. Sun, B. L. Shao, T. T. Zhou, and C. Q. Chen, *Materials Characterization*, vol. 56, no. 2, pp. 121–128, 2006.

[11] A. Deschamps, G. Fribourg, Y. Bréchet, J. L. Chemin, and C. R. Hutchinson, *Acta Materialia*, vol. 60, no. 5, pp. 1905–1916, 2012.

[12] A. Deschamps, Y. Bréchet, and F. Livet, *Materials Science and Technology*, vol. 15, no. 9, pp. 993–1000, 2013.

[13] A. Deschamps, F. Livet, and Y. Bréchet, *Acta Materialia*, vol. 47, no. 1, pp. 281–292, 1998.

[14] S. Esmaeili and D. J. Lloyd, *Materials Characterization*, vol. 55, no. 4–5, pp. 307–319, 2005.

[15] S. Esmaeili and D. J. Lloyd, *Acta Materialia*, vol. 53, no. 20, pp. 5257–5271, 2005.

[16] P. Sepehrband and S. Esmaeili, *Materials Science and Engineering A*, vol. 487, no. 1–2, pp. 309–315, 2008.

[17] S. Esmaeili, D. J. Lloyd, and W. J. Poole, *Acta Materialia*, vol. 51, no. 8, pp. 2243–2257, 2003.

[18] L. M. Brown and R. K. Ham, *Applied Science, London*, vol. 9, 1971.

[19] A. Deschamps and Y. Brechet, *Acta Materialia*, vol. 47, no. 1, pp. 293–305, 1998.

[20] J.W.Christian, *The Theory of Transformations in Metals and Alloys*. 1959.

[21] M. J. Starink, *Journal of Alloys and Compounds*, vol. 630, pp. 250–255, 2015.

[22] M. Perez, M. Dumont, and D. Acevedo-Reyes, *Acta Materialia*, vol. 56, no. 9, pp. 2119–2132, 2008.

[23] Haasen. P, *Physical Metallurgy*. Cambridge University Press, 1986.

[24] W. J. Poole, J. A. Seter, S. Skjervold, and G. Waterloo, *Metallurgical and Materials Transactions A: Physical Metallurgy and Materials Science*, vol. 31, no. 9, pp. 2327–2338, 2000.

[25] P. Sepehrband and S. Esmaeili, *Unpublished results*, 2007.

[26] A. Deschamps, G. Texier, S. Ringeval, and L. Delfaut-durut, vol. 501, pp. 133–139, 2009.

[27] D. Geuser, *applied crystallography*, vol. 44, pp. 343–352, 2011.

[28] N. Baghbanaghaie, *MASc thesis, University of Waterloo*, 2021.